In situ key aging parameter determination of a vehicle battery using only CAN signals in commercial vehicles

Applied Energy 314 (2022) 118932

Contents lists available at ScienceDirect

Applied Energy

journal homepage: www.elsevier.com/locate/apenergy

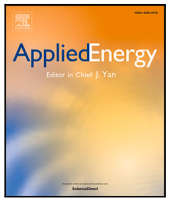

In situ key aging parameter determination of a vehicle battery using only CAN signals in commercial vehicles

Zeyang Geng *, Torbjörn Thiringer

Department of Electrical Engineering, Division of Electric Power Engineering, Chalmers University of Technology, 412 96 Gothenburg, Sweden

ARTICLE INFO

Keywords:
Batteries
Built-in testing
Impedance measurement
Vehicles

ABSTRACT

In this article, an on-line impedance measurement technique for a battery pack is demonstrated and proofed, using only the already existing sensors and accessible bus data in an electrified vehicle. A sufficient amount of AC harmonics in the DC-link current, for the identification purposes, is created in normal driving conditions. Fourier analysis is used to process the data and extract the impedance information. It is found that the proposed on-line method can accurately measure the battery pack impedance at a low frequency range (5 Hz to 10 mHz) with 40 Hz sampling frequency in the bus data. A key impedance value in the electrochemical impedance spectroscopy can be captured clearly in different conditions, which can be used to track the battery state of health. A recorded current waveform during an on-road test is reproduced by a state-of-art battery tester in a lab and the obtained results are compared with impedance values measured by a classic potentiostat. The results from the on-road test have an excellent agreement with lab measurements.

1. Introduction

Although prices are declining, batteries still remain to be one of the most expensive components in an electrified vehicle. In order to fully utilize the battery during its life in vehicles, it is important to monitor its performance [1,2]. There are two key features that need to be identified to estimate the state of health (SOH) of a battery: the remaining capacity and impedance. The remaining capacity of a battery can be fairly well estimated during the charging events if the vehicle is a plug-in hybrid electric vehicle (PHEV) or a battery electric vehicle (BEV). The impedance typically increases with battery aging which results in a reduced output power [3]. However, compared to the estimation of the battery pack's capacity, determination of its impedance is more complicated.

Common methods to estimate the battery pack impedance are using Kalman filtering (KF) [4,5] or adaptation algorithms [6,7] together with equivalent circuit models (ECMs) that consist of resistors and capacitors. A limitation for these methods is that the models and algorithms are detailed to a specific battery, and requires continuous tuning, for instance due to ageing. In addition, the simplified ECMs cannot represent the battery's nonlinear properties and thus the results are difficult to interpret with physical meanings.

Apart from estimation techniques, there is a great interest in studying how to perform a measurement of the battery impedance in the frequency domain, where models are not needed [8,9]. To measure the battery impedance accurately in a laboratory environment, the method Electrochemical Impedance Spectroscopy (EIS) is commonly applied, where current signals with different frequencies are injected. This method requires a dedicated potentiostat which is typically not available to a battery pack in an electric vehicle application. There have been attempts made to measure the battery pack's EIS via the harmonics in the electrical system [10], with the challenges that the results can deviate due to drifting, noise and narrow-band distortions [11]. In [12,13], dc–dc power electronics converters are manipulated to create harmonics injected into the battery. In [14] an electric motor was used to generate excitation signals and the impedance of a 12 V battery pack was measured from 1 Hz up to 2 kHz. However, in the literature mentioned above, the experiment has only been performed in lab environment with a controllable setup and the data acquisition system has a very high sampling frequency. Neither of the circumstances are available in a normal electric vehicle. [15] presented a study case where a vehicle was driven according to standard drive cycles to extract the battery impedance. The extracted information is used to estimate the state of charge of the battery pack with a circuit model and an extended Kalman filter. The estimated parameters in the circuit model varies significantly depending on the selected drive cycles and they give little information about the physical properties of the battery and are thus not suitable for the aging diagnostic purpose. Bohlen O. demonstrated a method to extract the impedance spectrum of a lead–acid starter battery in [16]. The accuracy and validity of the

* Corresponding author.
E-mail address: zeyang.geng@chalmers.se (Z. Geng).

https://doi.org/10.1016/j.apenergy.2022.118932
Received 16 July 2021; Received in revised form 7 February 2022; Accepted 9 March 2022
Available online 25 March 2022

proposed methodology was carefully analyzed, however the results did not provide a clear impedance trajectory so that a key value could be extracted.

To sum up, what is missing in available literature is a methodology and its proof of concept in real life regarding on-line measurement of battery pack parameters, which can be used in commercial vehicles, with the deficits regarding data acquisition, and provide key information of the battery state of health, through the determination of a key impedance value. The goal of this work is to demonstrate a proposed methodology through which this key aging factor can be identified using standard sensors available in commercial vehicles. This is achieved by driving a PHEV at various temperatures and states of charge. Data on the Controller Area Network (CAN) bus is collected during driving and processed by using Fourier analysis to extract the key parameter. Furthermore, an important target in this context is to verify the results in a laboratory environment with, a for this purpose dedicated instrument, i.e. a potentiostat to proof its validity. The proposed method is able to measure the EIS at a low frequency range down to 10 mHz and determine the sum of the ohmic resistance and charge transfer resistance, which is a key information for battery aging diagnostics [17,18]. This value can be tracked during driving throughout the electric vehicle lifetime whereas another aging feature, the capacity fading, can be tracked during charging.

The contribution with this article is thus that it demonstrates, in a real-life application, how a key impedance value of a vehicle battery can be found only using the data transmitted via a typically available standard CAN bus for aging diagnostics, which has not been published so far in scientific literature.

2. Theory

2.1. Electrochemical impedance spectroscopy (EIS)

During charge or discharge, a series of electrochemical processes occur inside the battery with different time constants. In Fig. 1, the electrochemical processes are illustrated with a transmission line structure, where R_s represents the resistance of the electron flow paths in the particles, Z_l reflects the mass transport of the electrolyte, U is the open circuit potential, Z_w is the Warburg impedance caused by the diffusion process inside the particle, R_{ct} is the charge transfer resistance caused by the charge transfer reactions, R_{film} is the additional resistance created by the solid electrolyte interphase (SEI) on the negative electrode and the solid permeable interface (SPI) on the positive electrode. C_{dl} is the double layer capacitance due to adsorption. The current flow in C_{dl} is a non-faradic process which is independent from the electrochemical reactions and therefore it is connected in parallel with Z_w, R_{ct} and R_{film}.

One example of an EIS measurement result and how it reflects the electrochemical processes is shown in Fig. 2. At a very high frequency range (kHz), the battery system shows an inductive behavior which is related to the wiring connections [19]. At 505 Hz, the inductive and capacitive behaviors in the system are balanced, and the battery impedance is purely resistive at this point. The impedance at this zero-crossing point is often called R_0, which includes the electronics resistance in the current collectors and electrodes, as well as the ionic resistance in the electrolyte. Since the electronic conductivity in the electrode is a few orders of magnitude higher than the electrolyte conductivity, R_s has a much smaller value than R_l. Therefore, R_0 is dominated by the electrolyte resistance in the separator $Z_{l,sep}$. With a decreasing frequency, the charge transfer reactions are pronounced and a semi-ellipse shape appears in the impedance plot as the result of a RC link connected in parallel. The width of the semi-ellipse is defined as R_1. This semi-circle is slightly pressed in the vertical direction since the double layer capacitor is a non-linear component [20] and it is merged from two semi-ellipses from the two electrodes. At a low frequency range (<1 Hz), the slowest process in the battery, the Li-ion diffusion in

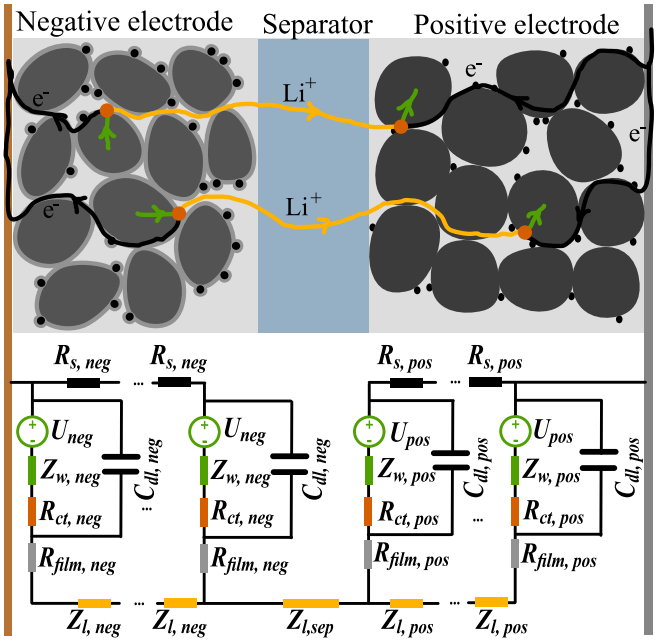

Fig. 1. Electrochemical processes inside the battery.

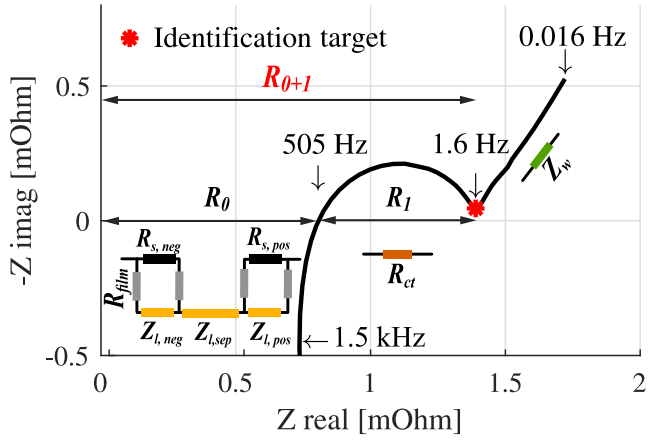

Fig. 2. The impedance of a Li-ion battery measured with a potentiostat by using EIS at 20 °C 50% SOC and how it can be interpreted with physical phenomena.

the particles, is visible in the EIS plot, the so called Warburg impedance. Besides the material and geometry, the battery EIS is also affected by temperature, current magnitude and direction, state of charge (SOC) and SOH. To demonstrate this, the impedance of the cell used in this work is measured by using EIS at different states of charge, from 100% to 0% with a step size of 10%, at different temperatures of 10 °C, 20 °C, and 30 °C. The results are presented in Fig. 3. The impedance dependency on SOC and temperature can be explained with an example of the charge transfer resistance. The charge transfer reaction can be described with the Butler–Volmer equation

$$j = j_0(exp\frac{\alpha_a F\eta}{RT} - exp\frac{-\alpha_c F\eta}{RT}) \quad (1)$$

and the charge transfer resistance at the particle surface is

$$R'_{ct} = \frac{\eta}{j} \quad (2)$$

where j is the charge transfer current density per surface area [A/m^2], j_0 is the exchange current density, α_a and α_c are the anodic and cathodic constant, F is the Faraday constant, R is the gas constant, T

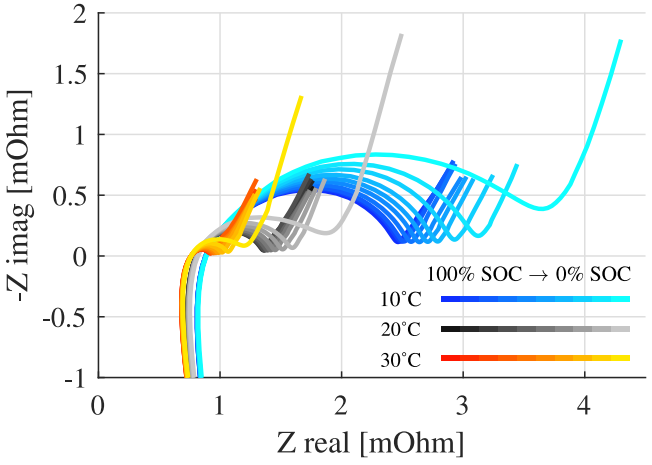

Fig. 3. The impedance of a Li-ion battery measured with a potentiostat by using EIS at different temperatures and states of charge, with a step size of 10% SOC. The results demonstrate how the temperature and SOC affect charge transfer resistance. The charge transfer resistance is higher at a low temperature and low SOC.

is temperature and η is the overpotential caused by the charge transfer reaction.

R_{ct} and temperature: When the battery is at its equilibrium state, i.e. zero net current on the macro scale, there is, however, current flows on the micro scale, but with the same magnitude in both directions. This current flow is called the exchange current density j_0. The exchange current density of lithium intercalation j_0 is

$$j_0 = F k_c^{\alpha_a} k_a^{\alpha_c} (c_{s,max} - c_{s,surf})^{\alpha_a} c_{s,surf}^{\alpha_c} c_l^{\alpha_a} \tag{3}$$

where k_c and k_a are the cathodic and anodic rate constants, $c_{s,max}$ is the maximum concentration in the particle (these three parameters are material related properties), $c_{s,surf}$ is the Li-ion concentration at the particle surface which is SOC dependent and c_l is the Li-ion concentration in the electrolyte. The rate constants k_c and k_a are strongly affected by temperature, following the Arrhenius equation. With higher temperature, k_a and k_c increase, and so does also j_0, which gives a lower charge transfer resistance (approximately the width of the semi-ellipse), as shown in Fig. 3.

R_{ct} and SOC: In addition to the temperature, j_0 is also affected by the Li-ion concentrations,

During discharge, the Li-ions flow from the negative electrode to the positive electrode and thus the Li-ion concentration at the negative electrode is decreasing, whereas it is increasing in the positive electrode. The concentration change will affect the exchange current density in (3) and it is reflected in the EIS measurement that the charge transfer resistance is higher at a lower SOC, as shown in Fig. 3. This behavior can be observed for all three temperatures. The calculation of j_0 in (3) assumes a lattice gas behavior in the electrode. With this simplification, the relationship between R_{ct} and SOC should be a U-shape [21]. However, in reality the graphite has a staging process during intercalation which does not follow (3) strictly.

R_{ct} and current: The Butler–Volmer Eq. (1) describes an exponential function between the current j and the overpotential η and the charge transfer resistance at the particle surface R'_{ct} is the slope of this function. Naturally R'_{ct} decreases as the current magnitude increases. Apart from the magnitude, the current direction also plays a role. α_a and α_c describes how easy it is to drive the process in one direction or the another one. Often these two values are not equal which means it can be more difficult to drive the current (higher resistance) during charge or discharge.

In a lab environment, an EIS measurement is performed at equilibrium state and the DC current component is zero in the perturbation signal, which keeps the battery system in the same state regarding SOC and temperature. However in this work, the EIS is measured when the vehicle is driving, meaning both the SOC and the temperature are varying during the measurement. Therefore it is important to limit the length of the data used to extract the impedance so that the battery state does not vary too much during the selected time period.

2.2. EIS and battery aging

The ending point of the semi-ellipse (1.6 Hz in Fig. 2) is the targeting point (the value is defined as R_{0+1} as shown in Fig. 2) in this work, since this point is distinguished in the EIS plot and it can be used to track the SOH of the battery, as motivated below.

In the majority of the commercial Li-ion batteries, graphite is used as the negative electrode which is outside of the electrolyte stability window and thus there is SEI and SPI forming between the graphite particles and the electrolyte. It is both a protection layer to keep the battery functional whereas it is one of the main aging mechanisms in batteries [22] as it consumes cyclable Li-ions. The resistances caused by the SEI and SPI are represented as $R_{film,neg}$ and it is increasing with aging as the SEI and SPI film thicknesses grow [23]. This information is reflected in R_{0+1}, the chosen identification point in this work.

Apart from the SEI and SPI formation, another main aging mechanism is structural degradation and particle isolation that leads to a loss of active materials [24]. As it is shown in Fig. 1, the electrode material has a porous structure to increase the contact surface area between the particle and the electrolyte. In (2), the unit of R'_{ct} is [$\Omega \cdot m^2$] and the area here is the total surface area of the particles instead of the electrode area. The translation between R'_{ct} and R_{ct} in the EIS plot is

$$R_{ct} = \frac{R'_{ct}}{A d S_a} \tag{4}$$

where A is the electrode area, d is the electrode thickness and S_a is the specific surface area, which is the total surface area per volume. During battery aging, the loss of active materials will result in a smaller S_a and thus larger R_{ct}, which is part of the identification value R_{0+1} as well. Moreover, other aging mechanisms such as current collector corrosion, lithium plating and electrolyte dry out causing decreased ionic conductivity [25] can also lead to an increase in R_{0+1}.

One example of how the targeting point R_{0+1} can be related with the battery SOH is shown in Fig. 4. A battery cell (the same type as the other cells used in this work) has been cycled with +2C/-2C constant current between 3 V and 4 V under 20 °C. Reference performance tests (RPTs) have been performed regularly which are indicated as the dots along the aging curve. In each RPT, the EIS of the battery cell is measured with a sinusoidal sweep from 50 Hz to 0.05 Hz. At the beginning of life (BOL), the battery has 100% capacity and the target point has a real part of the impedance of 1.3 mOhm. As the capacity fades to 90%, the target point R_{0+1} increases to 1.5 mOhm.

To sum up, the value R_{0+1} in Fig. 2 is a useful input for battery SOH diagnostic and therefore, the target in this work is to be able to measure this value in a complete battery pack in a vehicle with only on-board hardware.

2.3. Identification signals in the frequency domain

The identification target in Fig. 2 corresponds to the system response at 1.6 Hz. However, this specific frequency varies with temperature and SOC level. The reason is that the frequency value is related to the time constant of the RC links in Fig. 1 and thus affected by the charge transfer resistance. Based on the results in Fig. 3, the frequency values when $Z_{cell,real} = R_{0+1}$ at different temperatures and SOC levels are summarized in Fig. 5. The temperature shown in Fig. 5 is the cell surface temperature measured with a type K thermocouple. The frequency step here is determined by the potentiostat software setting when performing the EIS, which is 10 measurement points per decade. To measure R_{0+1} at the target point, a non-parametric

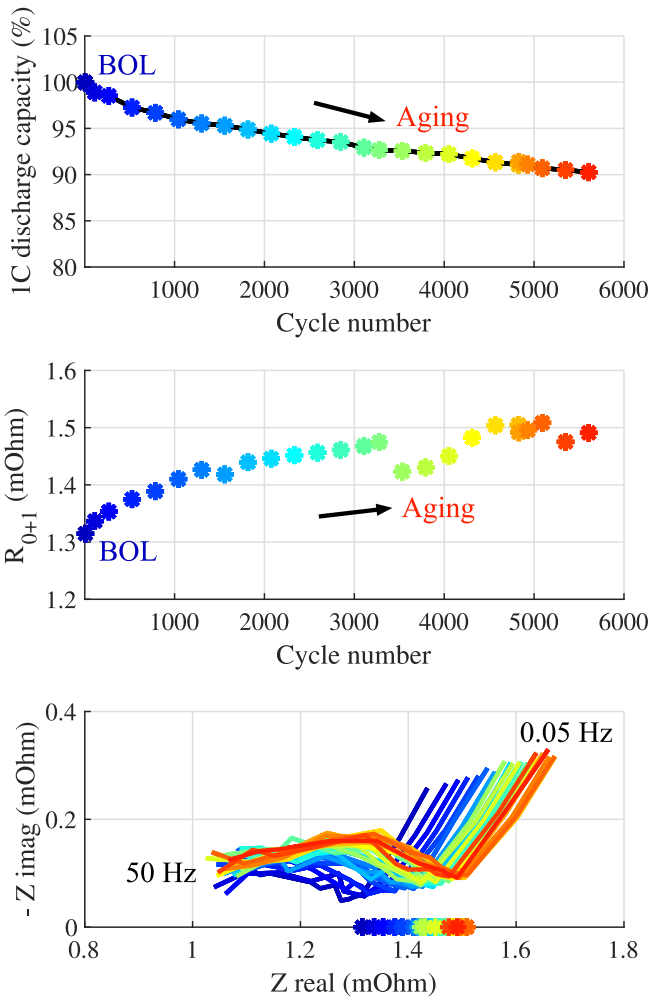

Fig. 4. The identification target R_{0+1} increases with the battery aging and it is a useful information for the SOH diagnostic. The impedance is measured with a regular battery tester by applying a series of manually created sin-waves.

system identification method is used in this work, which does not require a model of the system. In this method, the identification signal shall contain AC components whose frequency cover the required range. There are a few options for the identification signals for this purpose.

Sinusoidal and multisine signals: The classical identification signal for EIS measurement is a series of sine waves with different frequencies sweeping through the frequency range of interest, typically from high frequency to low frequency. The impedance at each individual frequency can be calculate as

$$Z(f) = \frac{U(f)}{I(f)} \tag{5}$$

where f is the frequency. Another options is to combine a number of sinusoidals into a multisine signal to speed up the measurement, which has been implemented in commercial potentiostats. In a multisine measurement, the input and output signals can be decomposed into harmonic components using Fourier analysis

$$F = F_0 + \sum_{n=1}^{\infty} \sqrt{2} F_n \sin(n\omega t + \phi_n) \tag{6}$$

where F is the current or voltage waveform, and $\omega = 2\pi f$ is the angular frequency. Then the impedance at each frequency is calculated with (5). Both sinusoidal and multisine signals require dedicated equipment to generate and measure the signals, which is not available in the vehicles

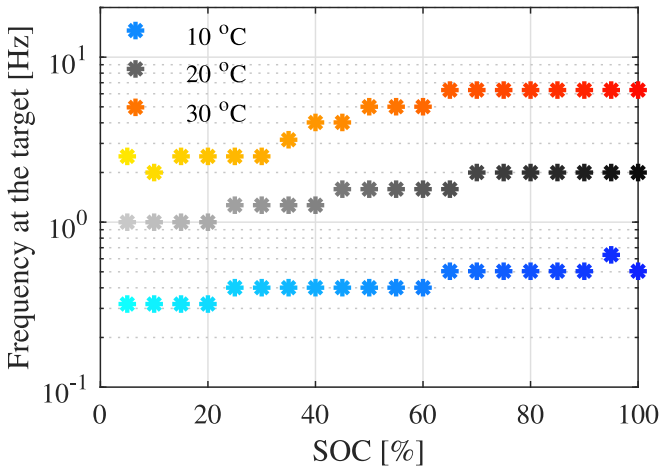

Fig. 5. EIS measured in the lab environment to demonstrate the temperature and SOC dependency. Observe that the potentiostat provided results in discrete steps.

on the market. Therefore they are not suitable for the purpose of this work.

Pseudo-random binary sequences (PRBS): PRBS is a band-limited white noise which is often used in system identification [26]. It can be designed with different bits and clock frequencies to cover a desired frequency range. In a previous study [27] it has been shown that PRBS can be used the measure the battery EIS with an excellent agreement with classical EIS measurement. One example of an 8 bit PRBS generator is shown in Fig. 6(a) and the AC component of this PRBS with 40 Hz clock frequency f_c is shown in Fig. 6(b). The usable frequency range is defined by the 3 dB bandwidth, ranging from $f_{min} = f_c/(2^8 - 1) = 0.16$ Hz to $f_{max} = f_c/3 = 13$ Hz. With this designed PRBS, it covers the target frequency range 0.3 Hz–6 Hz in Fig. 5. A PRBS signal is easier to create than sine waves since it only contains binaries. However, it is still difficult to generate a binary sequence current with clear steps to the battery pack in a vehicle, due to the limitation of acceleration and braking. Moreover, the sampling frequency has to be at least a few times higher than the clock frequency 40 Hz to achieve a decent result. Such a sampling frequency is possibly achievable within the internal control unit of the battery management system but cannot be reached in the network outside.

During driving: As long as a signal contains certain harmonics in the frequency domain, this signal can be used for system identification, which applies to a real driving cycle as well. In this work, short segments are selected in driving cycles to extract the battery EIS, especially to identify R_{0+1} in Fig. 2. The lengths of the segments are limited so that the SOC and temperature do not vary too much, as described earlier. Fourier analysis (6) is used for data processing. During the driving cycle measurement, only on-board equipment is used and the signals are obtained from the CAN (Controller Area Network) bus. The date from the CAN bus are resampled with an average sampling frequency before performing Fourier analysis.

3. Test objects and environment

The experiment in this work consists two parts: on-line measurements in a test vehicle and EIS verification in a laboratory. The vehicle is driven on a test track at various temperatures and SOC levels. One of the current patterns recorded in the vehicle during driving is reproduced on a single cell in a controlled lab environment to verify the results.

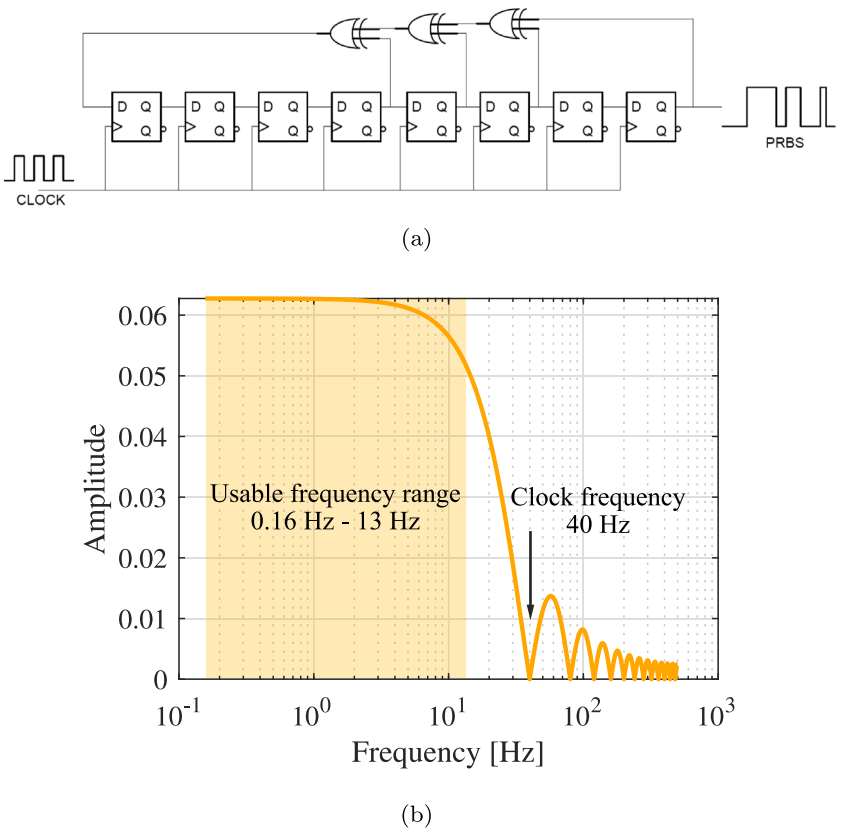

Fig. 6. (a) An 8 bit PRBS generator example. (b) AC components of the 8 bit PRBS.

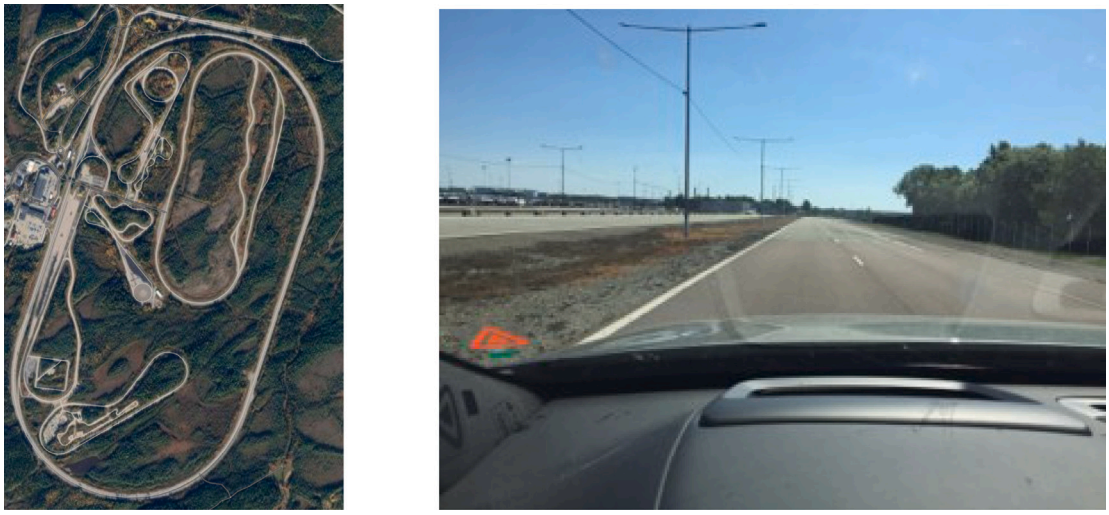

Fig. 7. (a) A satellite view of the test track. (b) The view from the vehicle during the experiment.

3.1. Test vehicle and track

A plug-in hybrid electric vehicle is used as test vehicle, which can drive about 40 km purely electrically. The battery pack in the vehicle is configured to be 96s1p (96 cells in series and 1 in parallel) and it consists of 6 modules with 16 pouch cells in each module. Each cell has a capacity of 26 Ah and the detailed information is described in [28]. The battery pack is equipped with a water cooling system to regulate the battery temperature. The functionality of the battery management system (BMS) in the test vehicle is the same as what exists in this type of vehicle on the market, without modification. The used vehicle, was fairly new and not heavily used, so the battery can also be considered as fairly new. This was also confirmed when comparing the results with new cells of the same type as used in the vehicle.

During the on-line measurement, the CAN bus data is acquired through the OBD (On-board diagnostics) connector, which is mandatory to be installed in vehicles in most countries. The messages on the CAN bus are event triggered instead of with a fixed schedule and therefore the time interval between each message is not constant. The average sampling frequency of the signals is 40 Hz, and this sampling

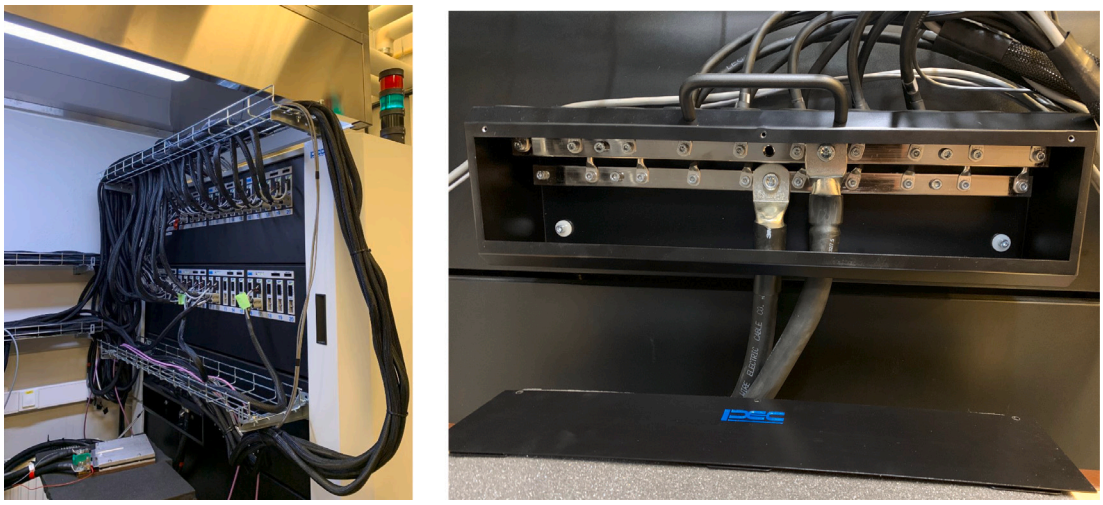

(a) (b)

Fig. 8. (a) PEC ACT0550 tester, the current range of a single channel is 50 A. (b) Five channels from the tester are paralleled to extend the current range to 250 A.

frequency limits the maximum frequency where the battery information can be extracted. All the signals (voltage, current and temperature) are measured with the on-board sensors in the battery packs. However, the voltage and current signals are scheduled in separate messages on the CAN bus therefore the signals of the voltage and current are not exactly synchronized. No additional equipment has been used for the experiment other than what is already available in the vehicle and can thus easily be used by vehicle manufacturers.

The tests are conducted on a test track as shown in Figs. 7(a) and 7(b), by both professional test drivers and the authors. Various driving styles are explored by using the brake and accelerator pedal to create AC harmonics on the battery DC bus. The experiment are performed both in winter and summer to create different ambient temperatures. However due to the mild winter conditions, a cooling room is used to cool the complete vehicle to a low temperature (−10 °C).

3.2. Laboratory experimental set-up

Since it is not applicable to measure the EIS of the battery pack with another method to compare with the results in this work, an experiment is conducted on a single cell in a controlled laboratory environment to verify the proposed methodology. One of the recorded current profile from the driving is recreated by a battery tester PEC ACT0550 (±0.005% FSD (Full Scale Deviation) for the voltage measurement and ±0.03% FSD for the current measurement), as shown in Fig. 8(a). Each channel in the ACT0550 can supply a maximum current level of 50 A whereas the peak current during driving can exceed 200 A on a single cell. Therefore 5 channels from the tester are paralleled to a bus bar to extend the current range to 250 A, as shown in Fig. 8(b). The cables at the high current side are capable to handle 500 A and only half of capacity of the parallel kits is used.

The battery cell used is a 26 Ah Li-ion pouch cell, which is the same type of battery as the ones in the test vehicle. The material of the positive electrode is a mixture of $LiNi_{0.3}Mn_{0.3}Co_{0.3}O_2$ and $LiMn_2O_4$, and the negative electrode is graphite. Further details about the investigated cell can be found in [28]. The cell is located in between two aluminum plates with a fixed distance to emulate the environment in the battery pack, as shown in Fig. 9. To secure a proper impedance result, a 4-wire connection is used and the voltage sensing points are located directly on the battery tab to exclude the resistance in the rest of the system. The battery surface temperature is monitored with a type K thermocouple temperature sensor.

To validate the result obtained from the test track driving, the current from a drive case is reproduced in a laboratory environment without scaling, and applied to a single cell as shown in Fig. 9. A standard EIS with 1 A RMS current is conducted by a state-of-art potentiostat, GAMRY Reference 3000 (accuracy < 1% for the impedance measurement), on the same cell at the same condition as the reference to verify the results from the drive case. Besides the signal waveform, the main difference between the test track on-line measurement and laboratory EIS is the current magnitude. As explained previously in Section 2, the charge transfer resistance is lower under a high current, therefore an EIS with 10 A RMS current is measured to check how the current magnitude affects the EIS measurement results. To reach a higher current amplitude, the PEC ACT0550 is used to implement the PRBS method described in Fig. 6 with both 10 A and 100 A magnitude, and the drive case, where the RMS current is around 100 A. In total 5 identification signals are applied: 1 A and 10 A (RMS value) EIS by GAMRY Reference 3000 with booster, 10 A PRBS, 100 A PRBS and recorded current from test track driving by the PEC ACT0550 with the parallel kit.

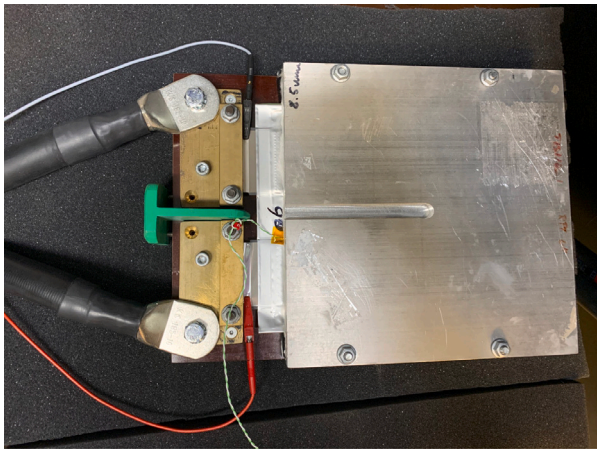

Fig. 9. Battery cell tested in laboratory environment with 4-wire connection.

4. Results and analysis

4.1. Results from various drivings

The test vehicle was driven for more than 50 times, from fully charged to discharged, at different temperatures. Short segments are

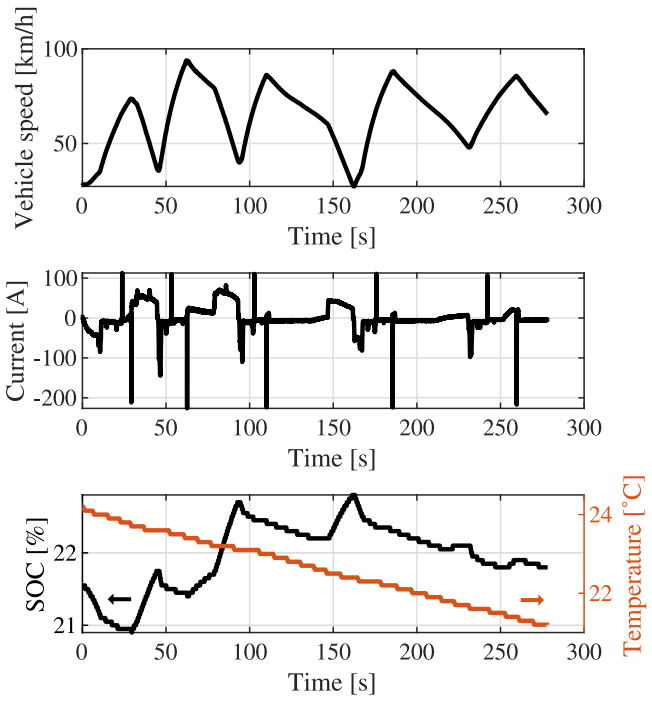

Fig. 10. The raw measurement data from CAN bus in drive case A at 22% SOC and 23 °C, with cooling system activated.

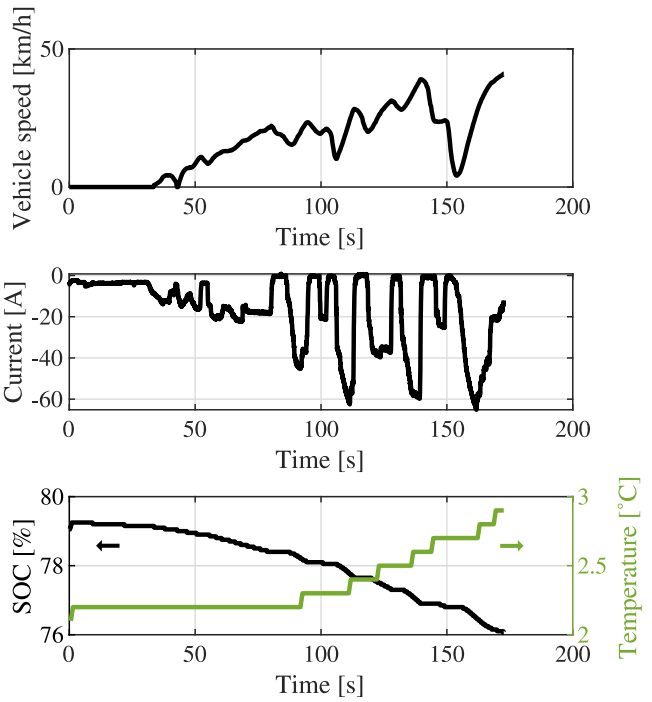

Fig. 11. The raw measurement data from CAN bus in drive case B at 78% SOC and 2.5 °C.

cut from the log files for data processing, with the criteria of maximum 5% SOC change and 3 °C temperature change, so that the battery pack impedance does not change significantly within one segment. In total 47 segments were processed, and from 25 segments, clear impedance trajectories can be extracted. When the test conditions are similar, the impedance extracted from different test cases show a good consistency, therefore only three representative cases are selected, shown in Fig. 10 (case A: 22% SOC, 23 °C), Fig. 11 (case B: 78% SOC, 2.5 °C) and Fig. 12 (case C: 21% SOC, −10 °C).

The vehicle used in the experiment is a hybrid plug-in vehicle and depending on the operation condition, the electric motor or the combustion engine or sometime both will be activated to operate the vehicle. The current is negative for discharge (driving) and positive for charge (regenerative braking or charged by the combustion engine). The temperature in the battery pack increases due to losses, as shown in Figs. 11 and 12. When the temperature reaches a certain limit, the battery management system (BMS) will activate the cooling system to cool down the battery, which is the case in Fig. 10.

During driving, the acceleration and brake pedals are used to create harmonic components on the battery DC side. The average sampling frequency is 40 Hz with asynchronous current and voltage samples since they are in separate CAN messages.

In the data processing part, a moving window with half of the signal length is used in the FFT (Fast Fourier transform). The impedance value is selected only when the frequency is above 0.01 Hz and the voltage amplitude is higher than a threshold at the corresponding frequency. The threshold value is tuned to reduce the impact of noises while obtaining a sufficient amount of data. The maximum identification frequency is around 5 Hz, depending on the test case. At this point, the results contain many frequencies and are therefore hard to visualize. To obtain a clear impedance trajectory, the results are partitioned evenly into 25 bins with the MATLAB command *histcounts*. The partition into bins is based on the natural logarithm of the frequency, therefore dividing a frequency range of 0.01 Hz to 5 Hz into 25 bins roughly corresponds to 10 bins per decade. This frequency resolution is similar as what is normally used in the potentiostat setups in a laboratory environment. With this frequency resolution, the R_{0+1} value can differ around

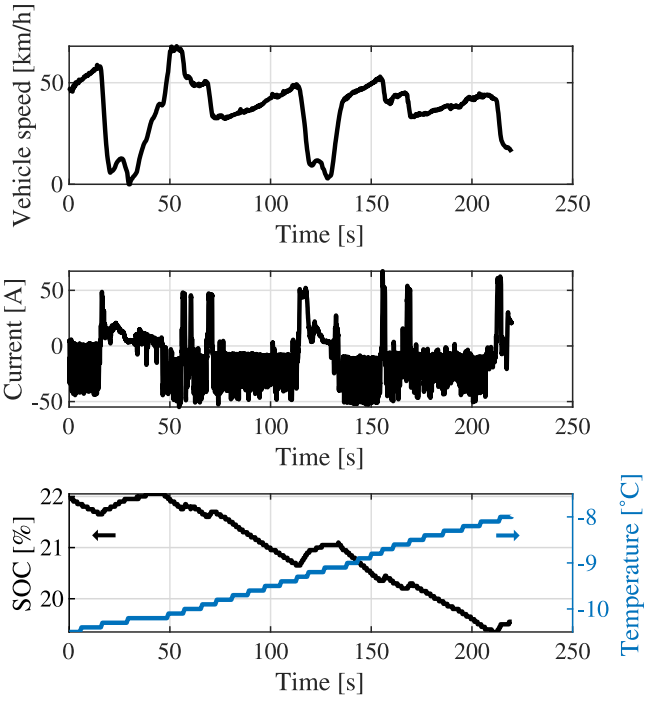

Fig. 12. The raw measurement data from CAN bus in drive case C at 21% SOC and −10 °C.

4 mOhm (3%), calculated with the R_{0+1} neighboring value in Fig. 2. A finer frequency step can be used in theory, but the introduced noise can reduce the visibility of the impedance appearance. After the partition, the mean value in each bin is then calculated with *accumarray*. With the procedure described above, the final results present an impedance trajectory which resembles the lab EIS measurement. The signature value R_{0+1} can then be identified when the imaginary part reaches

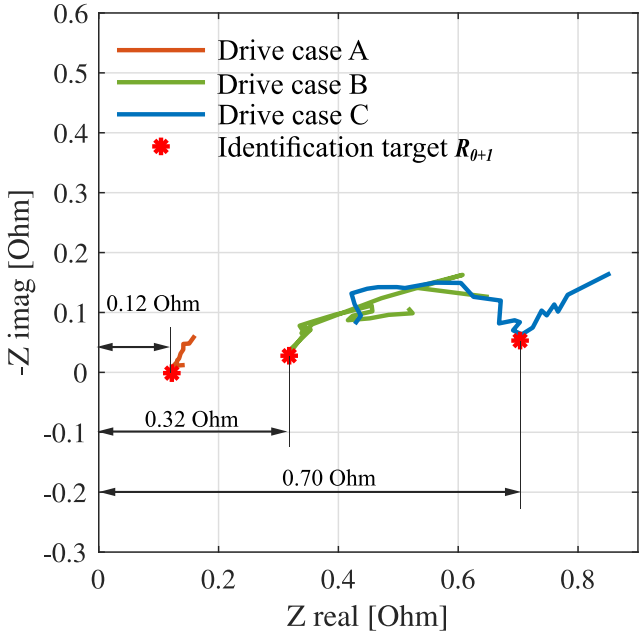

Fig. 13. EIS plot of the battery pack computed directly using the onboard data in drive case A, B and C. The identification target R_{0+1} can be captured as Z_{real} when $|Z_{imag}| = \min(|Z_{imag}|)$.

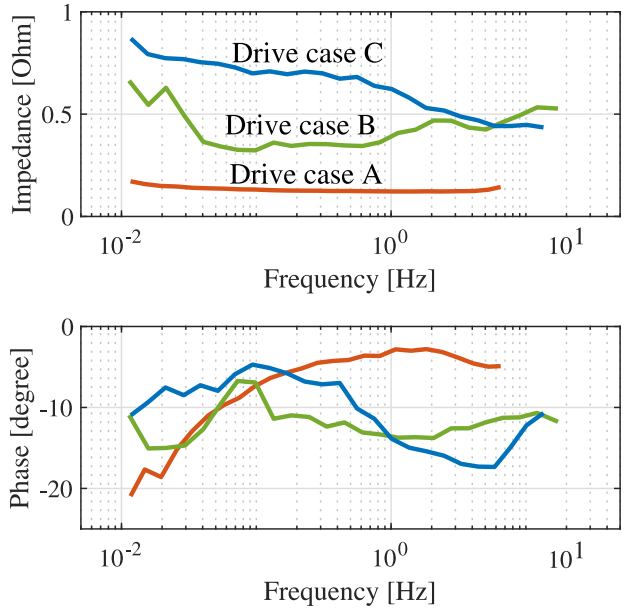

Fig. 14. Bode plot of the battery pack impedance extract from drive case A, B and C.

its minimum absolute value, regardless which frequency it is located. The advantage of this process is that it is a non-parametric approach, meaning that it does not dependent on the system states and characters, i.e., temperature, SOC, and SOH. As long as the signature point is located within the frequency range between 0.01 Hz and 5 Hz, the R_{0+1} value can be found in the EIS Nyquist plot. With a known SOC and temperature, the SOH can therefore be tracked with the R_{0+1} value.

The extracted battery pack impedance is shown in Figs. 13 and 14. Although it is not obvious in the bode plot in Fig. 14, the ending point of the semi-circle is distinguished in the EIS plot in Fig. 13. The identification target R_{0+1} in Fig. 2 can be captured as Z_{real} when $|Z_{imag}| = \min(|Z_{imag}|)$, despite different qualities from different drive cases. The result obtained from test track driving are summarized

Table 1
Identified R_{0+1} with driving cycles in different conditions.

Drive case	R_{0+1}
Drive case A: 22% SOC, 23 °C	0.12 Ohm
Drive case B: 78% SOC, 2.5 °C	0.32 Ohm
Drive case C: 21% SOC, −10 °C	0.70 Ohm

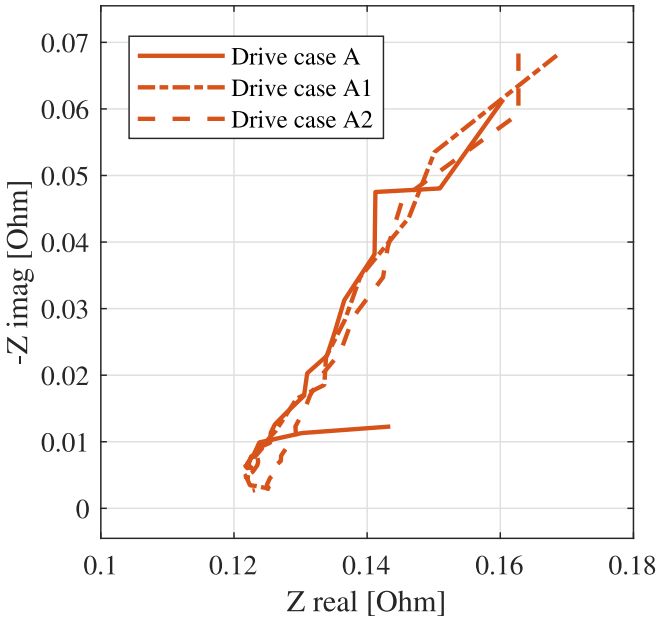

Fig. 15. EIS plots of a battery pack obtained from three separate drive cases with similar temperatures and SOC levels.

in Table 1. It shows that the value R_{0+1} is strongly affected by the temperature. In a cold climate −10 °C, R_{0+1} is almost 6 times higher than the value at 22 °C.

The repeatability of the proposed methodology is demonstrated in Fig. 15, with two additional cases A1 and A2 where the battery pack has similar temperature and SOC as in Case A. The battery pack impedance is the lowest in these cases and thus the most challenging to identify. These three cases are independent from each other, while still providing consistent results. The R_{0+1} obtained from three drive cycles are 0.123 Ohm, 0.125 Ohm and 0.123 mOhm. The spreading is within 2 mOhm, 1.6%. In the example of a mild aging test in Fig. 4, the cell impedance increase is around 15% per 10% SOH change. For the same type of cell used in this work, the impedance increase can be up to 45% when the cell reaches its end of life [28], which should be able to be tracked with the proposed method.

To study the impact of the asynchronous and uneven sampling, an investigation is performed as shown in Fig. 16. A synthetic input signal is superposed with sinusoidal waves at 6 frequencies: 0.1 Hz, 0.2 Hz, 0.5 Hz, 1 Hz, 2 Hz, and 5 Hz, covering the frequency range of interest. The ideal output signal is from a 3 Ohm resistor. The ideal input and output signals are re-sampled with the actual time vectors obtained from the vehicle CAN bus, which are asynchronous and uneven. It can be noted that the average sampling speed is 40 Hz for the current signal and 50 Hz for the voltage signal. The simulated input and output signals are then re-sampled with 40 Hz and used to perform FFT calculation. Since there are only 6 frequencies injected, only 6 points can be identified, which are selected and marked as the red dots. However, the routine identifies all possible frequencies, forming the black lines in the right figures which are noises. Compared with the true system, a slight error in the identified system is notable at 5 Hz, which is 0.2 Ohm, 6.7% higher than the true value. The phase is not strongly affected by the sampling for all studied frequencies.

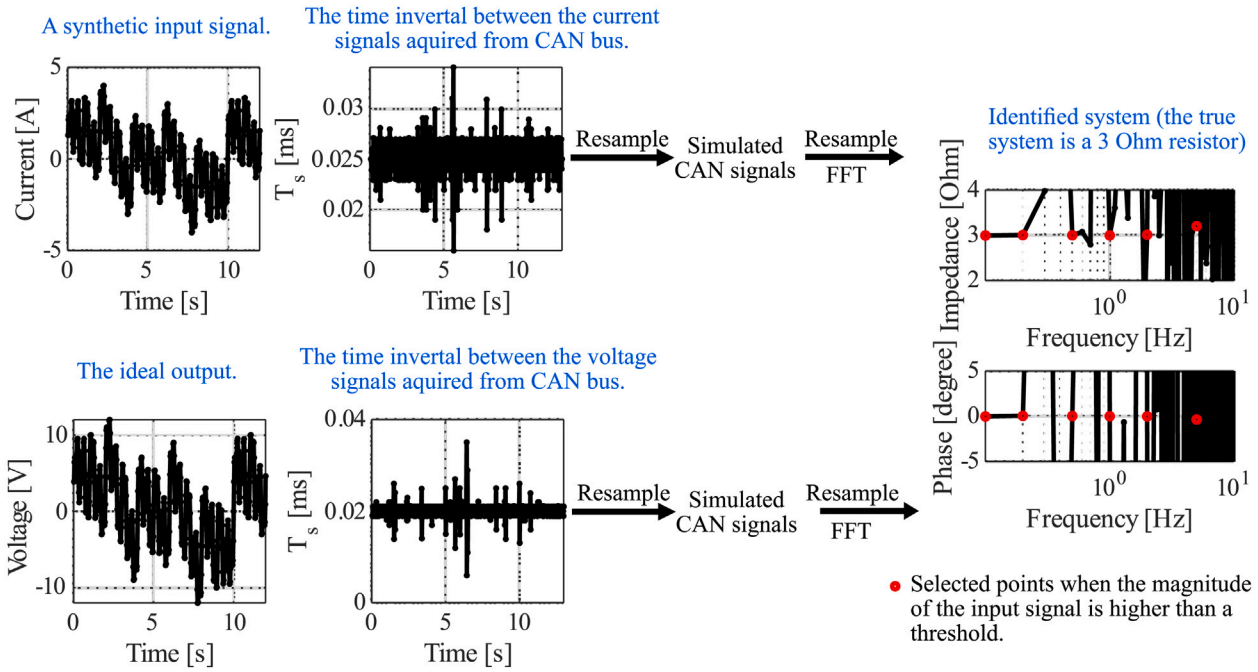

Fig. 16. Investigation about the impact of the asynchronous and uneven sampling of CAN signals.

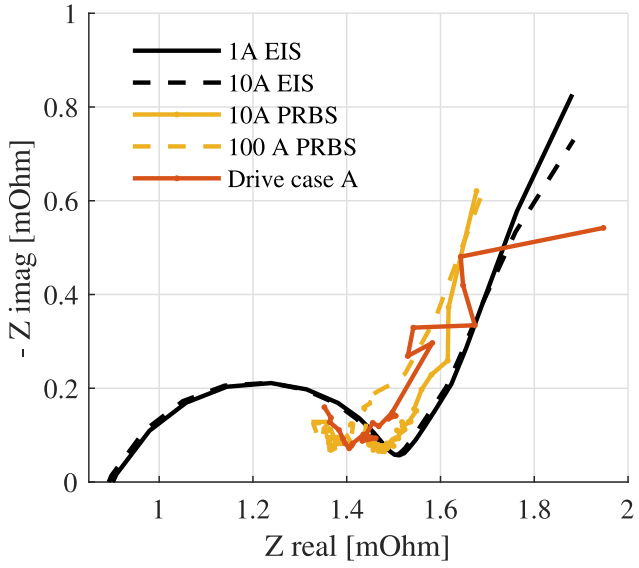

Fig. 17. EIS plot of a single battery cell measured with different methods, with a good agreement (22% SOC, room temperature).

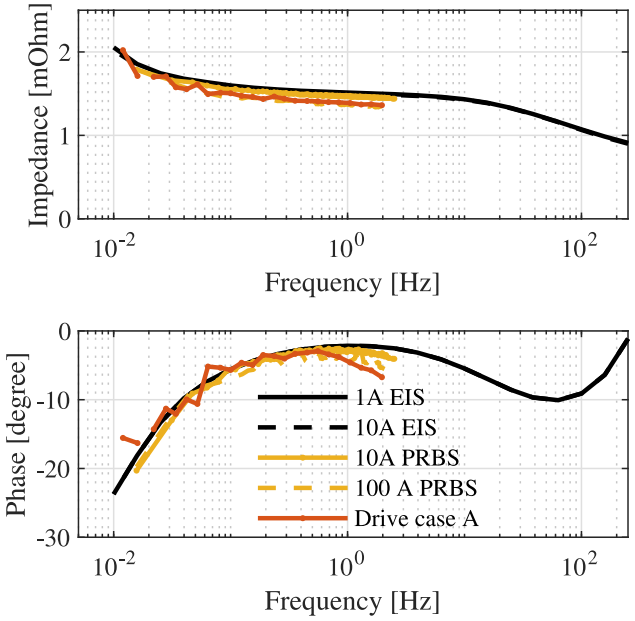

Fig. 18. Bode plot of a single battery cell measured with different methods (22% SOC, room temperature).

4.2. Lab verification

To validate the result obtained from the test track driving, the current in case A (Fig. 10) is reproduced in a lab environment without scaling and the it is compared with other identification methods described in 2.3. The results are presented in Figs. 17 and 18. It shows that the test track driving provides in principle the same result as a classic EIS-sweep.

The values of R_{0+1} obtained by the different methods and the difference are listed in Table 2. The values obtained by the signals with a higher current amplitude is slightly lower, which is expected and can be explained by (1). This difference is also affected by temperature. Although all 5 measurements are all performed under the same ambient temperature, a higher current creates higher losses and thus lead to a slightly higher temperature. Since the battery cell setup has a rather large thermal constant and the measurement time is short, the temperature during the driving cycle measurement is only 0.5 °C higher than the temperature during the EIS measurement. However, the battery impedance is very sensitive to temperature, as shown in Fig. 2 and the slight temperature difference can still affect the final result.

The signature value R_{0+1} of a single cell obtained with drive case A is 1.048 mOhm. A battery pack consisting of 96 such cells in series is expected to have a R_{0+1} value of 0.148 Ohm, counting 10% contribution from the bus bars. This value is slightly higher than the value of the battery pack in the test vehicle, 0.12 Ohm. This deviation can be explained with the differences in cell conditions as well as the

Table 2
Identified R_{0+1}. Besides the measurement noise and equipment accuracy, the differences are also due to the temperature and current magnitude.

Method	R_{0+1}	Difference
GAMRY 1 A EIS	1.512 mOhm	Reference
GAMRY 10 A EIS	1.503 mOhm	−0.6%
10 A PRBS	1.480 mOhm	−2.1%
100 A PRBS	1.363 mOhm	−9.8%
Test track driving $I_{RMS} = 21$ A	1.408 mOhm	−6.9%

measurement systems. For the single cell used in the laboratory, the cell surface temperature is around room temperature 25 °C. For the battery pack in the test vehicle, the temperature signal is reported from the BMS as the average temperature of the pack. With a series cooling circuit, the temperatures of the cells inside the pack can vary with a few degrees, which can affect the total pack impedance. Moreover, the cell in the lab and cells in the pack have different states of health which can affect the results as well. Besides different cell conditions, the differences in the measurement systems can lead to a deviation as well. The accuracy of the lab equipment is ±0.005% FSD (Full Scale Deviation) for the voltage measurement and ±0.03% FSD for the current measurement. The accuracy of the on-board sensors is unknown but a lower performance than the lab equipment can be expected. Another reason is that the current and voltage signals are sampled synchronously in the lab whereas the current and voltage signals are in separate CAN messaged in the vehicle and this can introduce a phase shift in the signal. Nevertheless, without any extra equipment, the on-board system can still provide a sufficient result to identify R_{0+1} which is a valuable information for SOH diagnostics.

With the proposed approach, the key impedance value of a EV battery pack can be extracted with only on-board sensors and CAN-bus data during driving at different temperatures and states of charge. Besides its good robustness, the repeatability of the method is verified with three separate cases under similar conditions shown in Fig. 15, with a maximum spreading of 1.6%. This is considered to be of high consistency compared with what was reported in literature, for example [16], where the deviation of the obtained impedance value is around 5%. One selected drive case is also repeated and verified in a laboratory environment with high accuracy equipment. The key impedance value of a single cell obtained with a drive cycle is 0.1 mOhm (6.9%) lower than what is measured with a potentiostat, despite the different order of magnitude of the input current.

The proposed method is a non-parametric identification method, meaning that it does not dependent on the system states and characters. The signature value R_{0+1} can be captured with typical CAN signals, as long as it is located within a frequency range between 5 Hz and 0.01 Hz, which is the case when looking into literature describing battery ageing behavior for automotive applications, for instance in [19]. This makes that, down to the 80% aging limit, which is typically proposed as the lower limit for batteries used in vehicles, the method should be possible to implement and provide information for aging diagnostics.

5. Conclusion

In this paper, an on-line technique for determining the key impedance value for aging diagnostics, including the ohmic resistance and charge transfer resistance, has been presented. Measurements have been performed with a plug-in hybrid electric vehicle with only on-board hardware in various conditions. In addition, experiments on a battery cell, of the same brand as in the vehicle battery, has also been conducted in a controlled laboratory environment to check the validity of the presented method. The results show that the key impedance value can be clearly captured during on-road driving with standard vehicle CAN bus data. In a laboratory environment, the recorded current signals from the vehicle is reproduced and the extracted impedance value agrees very well with the values obtained from other measurement techniques, with only 6.9% difference. The minor difference between the result of the test track driving and the result from classic electrochemical impedance spectroscopy measurement is due to different current magnitude, slightly different temperature, sensor accuracy and possibly sampling synchronization.

When it comes to future work, the dependencies of R_{0+1} on different factors such as dc current, SOC, SOH and on how the measurement accuracy depends on current and voltage noise, could be further investigated. Another suggested step is to track this key impedance value throughout the lifetime of a battery pack in an electrified vehicle to further enhance the SOH diagnostic function.

CRediT authorship contribution statement

Zeyang Geng: Conceptualization, Methodology, Software, Validation, Writing - Original Draft, Visualization, Writing – review & editing. **Torbjörn Thiringer:** Conceptualization, Methodology, Supervision, Writing – review & editing, Resources, Funding acquisition.

Declaration of competing interest

The authors declare that they have no known competing financial interests or personal relationships that could have appeared to influence the work reported in this paper.

Acknowledgments

The authors would like to thank Energimyndigheten and Volvo Car Corporation for the financing of this work. In particular we would like to thank Andreas Andreasson, Johan Fridner and Robert Eriksson at Volvo Car Corporation for arranging a test vehicle to borrow.

References

[1] Stockar S, Marano V, Canova M, Rizzoni G, Guzzella L. Energy-optimal control of plug-in hybrid electric vehicles for real-world driving cycles. IEEE Trans Veh Technol 2011;60:2949–62. http://dx.doi.org/10.1109/TVT.2011.2158565.
[2] Enthaler A, Gauterin F. Significance of internal battery resistance on the remaining range estimation of electric vehicles. In: 2013 international conference on connected vehicles and expo. IEEE; 2013, p. 94–9.
[3] Swierczynski M, Stroe D-I, Stan A-I, Teodorescu R, Laerke R, Kjaer PC. Field tests experience from 1.6 MW/400 kWh Li-ion battery energy storage system providing primary frequency regulation service. In: IEEE PES ISGT Europe 2013. IEEE; 2013, p. 1–5.
[4] Plett GL. Extended Kalman filtering for battery management systems of LiPB-based HEV battery packs - Part 1. Background. J Power Sources 2004;134:252–61. http://dx.doi.org/10.1016/j.jpowsour.2004.02.031, URL: <Go to ISI>://WOS:000223209700012.
[5] He H, Xiong R, Guo H. Online estimation of model parameters and state-of-charge of LiFePO4 batteries in electric vehicles. Appl Energy 2012;89:413–20.
[6] Chen Z, Mi CC, Fu Y, Xu J, Gong X. Online battery state of health estimation based on genetic algorithm for electric and hybrid vehicle applications. J Power Sources 2013;240:184–92.
[7] Farmann A, Waag W, Sauer DU. Adaptive approach for on-board impedance parameters and voltage estimation of lithium-ion batteries in electric vehicles. J Power Sources 2015;299:176–88.
[8] Wang X, Wei X, Zhu J, Dai H, Zheng Y, Xu X, et al. A review of modeling, acquisition, and application of lithium-ion battery impedance for onboard battery management. ETransportation 2020;100093.
[9] Kuipers M, Schröer P, Nemeth T, Zappen H, Blömeke A, Sauer DU. An algorithm for an online electrochemical impedance spectroscopy and battery parameter estimation: Development, verification and validation. J Energy Storage 2020;30:101517.
[10] Piret H, Granjon P, Guillet N, Cattin V. Tracking of electrochemical impedance of batteries. J Power Sources 2016;312:60–9.
[11] Koch R. On-line electrochemical impedance spectroscopy for lithium-ion battery systems [Ph.D. thesis], Technische Universität München; 2017.
[12] Varnosfaderani MA, Strickland D. Online impedance spectroscopy estimation of a battery. In: 2016 18th European conference on power electronics and applications. IEEE; 2016, p. 1–10.
[13] Varnosfaderani MA, Strickland D. Online electrochemical impedance spectroscopy (EIS) estimation of a solar panel. Vacuum 2017;139:185–95.

[14] Howey DA, Mitcheson PD, Yufit V, Offer GJ, Brandon NP. Online measurement of battery impedance using motor controller excitation. IEEE Trans Veh Technol 2013;63:2557–66.
[15] Sockeel N, Ball J, Shahverdi M, Mazzola M. Passive tracking of the electrochemical impedance of a hybrid electric vehicle battery and state of charge estimation through an extended and unscented Kalman filter. Batteries 2018;4:52.
[16] Bohlen O. Impedance-based battery monitoring. Shaker; 2008.
[17] Wang X, Wei X, Dai H. Estimation of state of health of lithium-ion batteries based on charge transfer resistance considering different temperature and state of charge. J Energy Storage 2019;21:618–31.
[18] Rahimi-Eichi H, Baronti F, Chow M-Y. Online adaptive parameter identification and state-of-charge coestimation for lithium-polymer battery cells. IEEE Trans Ind Electron 2013;61:2053–61.
[19] Groot J. State-of-health estimation of Li-ion batteries: Cycle life test methods. Chalmers University of Technology; 2012.
[20] Zubieta L, Bonert R. Characterization of double-layer capacitors for power electronics applications. IEEE Trans Ind Appl 2000;36:199–205.
[21] Lindqvist D. Simulation of intermittent current interruption measurements on NMC-based lithium-ion batteries. 2017.
[22] Pinson MB, Bazant MZ. Theory of SEI formation in rechargeable batteries: Capacity fade, accelerated aging and lifetime prediction. J Electrochem Soc 2012;160:A243.
[23] Tröltzsch U, Kanoun O, Tränkler H-R. Characterizing aging effects of lithium ion batteries by impedance spectroscopy. Electrochim Acta 2006;51:1664–72.
[24] Barré A, Deguilhem B, Grolleau S, Gérard M, Suard F, Riu D. A review on lithium-ion battery ageing mechanisms and estimations for automotive applications. J Power Sources 2013;241:680–9.
[25] Petzl M, Kasper M, Danzer MA. Lithium plating in a commercial lithium-ion battery–A low-temperature aging study. J Power Sources 2015;275:799–807.
[26] Al Nazer R, Cattin V, Granjon P, Montaru M, Ranieri M. Broadband identification of battery electrical impedance for HEVs. IEEE Trans Veh Technol 2013;62:2896–905.
[27] Geng Z, Thiringer T, Olofsson Y, Groot J, West M. On-board impedance diagnostics method of Li-ion traction batteries using pseudo-random binary sequences. In: 2018 20th European conference on power electronics and applications. IEEE; 2018, p. P–1.
[28] Wikner E. Lithium ion Battery Aging: Battery Lifetime Testing and Physics-based Modeling for Electric Vehicle Applications [Ph.D. thesis], Department of Electrical Engineering, Chalmers University of Technology; 2017.